Geochemical Perspectives Letters

Global patterns of radiocarbon depletion in subsoil linked to rock-derived organic carbon

K.E. Grant[1,2*], R.G. Hilton[3], V.V. Galy[4]

OPEN ACCESS

https://doi.org/10.7185/geochemlet.2312

Abstract

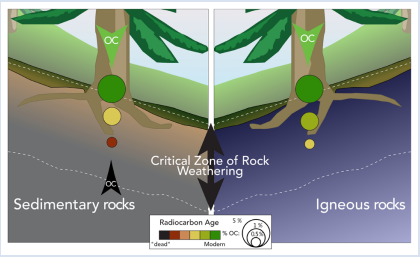

Organic matter stored in sedimentary rocks is one of the largest stocks of carbon at Earth's surface. The fate of this rock organic carbon (OC_{petro}) during weathering in soils influences the geological carbon cycle, and impacts soil radiocarbon content that is used to quantify soil carbon turnover. Here, we assess the potential contribution of OC_{petro} to soils, using a mixing model generated by a global dataset of soil radiocarbon measurements (^{14}C). Soils developed on sedimentary rocks (rather than on igneous substrate) have a paired OC content and ^{14}C values consistent with OC_{petro} input, giving rise to apparent increase in soil residence time. We call for renewed assessment of OC_{petro} input to soils, in terms of its impact on soil radiocarbon inventories, and its potential to release carbon dioxide.

Received 23 June 2022 | Accepted 6 March 2023 | Published 19 April 2023

Introduction

Sedimentary rocks cover 64 % of Earth's surface (Hartmann and Moosdorf, 2012). Within the upper 1 m, there are an estimated 1100 petagrams of carbon (PgC) present as radiocarbon (^{14}C) "dead" rock organic carbon (OC_{petro}) (Copard *et al.*, 2007), equivalent to the carbon stock in soils derived from the biosphere (Jackson *et al.*, 2017). When soil forms on sedimentary rocks, OC_{petro} is a "bottom up" input of carbon that can contribute to the soil OC pool, especially in deep soils with low OC concentrations (Hemingway *et al.*, 2018; Kalks *et al.*, 2021). While OC_{petro} could be widespread in soils developed on sedimentary rocks, observations come from only a handful of weathering profiles, including OC_{petro}-rich rocks, such as black shales which are not globally representative (Petsch *et al.*, 2001). In addition, estimates of global OC_{petro} surface exposure are based on upscaling from geological maps (Copard *et al.*, 2007), but this input has not been assessed in soil carbon studies. While there is widespread evidence for OC_{petro} in sediments from rivers around the world (*e.g.*, Galy *et al.*, 2015; Clarke *et al.*, 2017), we lack constraint on the input of OC_{petro} to soils.

Input of OC_{petro} to soil is important for two reasons. First, the exposure of rocks to weathering can drive OC_{petro} oxidation, releasing CO_2 and consuming O_2, with global emissions of CO_2 from OC_{petro} oxidation similar to those from volcanism (Petsch, 2014; Hilton and West, 2020). Second, OC_{petro} input can increase the mean age of soil OC based on radiocarbon (Agnelli *et al.*, 2002), used to quantify atmospheric CO_2 exchange by (Trumbore, 2000; Shi *et al.*, 2020). Soils slow the rapid degradation of "modern" plant-derived vegetation (OC_{bio}) through mineral and physical interactions, helping store OC_{bio} in soils over decades to millennia (Shi *et al.*, 2020). In the topsoil, the OC pool is dominated by plant and microbial organic matter and is generally ^{14}C-enriched (Shi *et al.*, 2020). In deeper soils (~>30 cm), recent studies (Mathieu *et al.*, 2015; He *et al.*, 2016; Shi *et al.*, 2020) show that ^{14}C-depleted ("old") OC is common around the world. These studies attribute "old" ^{14}C ages to an increase in OC-mineral interactions, as the clay content and mineral to organic ratio increase with depth and mineral surfaces can reduce the bioavailability and thus increase the persistence of OC_{bio} (Schmidt *et al.*, 2011). Soil C age distributions can have very long tails, with a small amount of old or ^{14}C-dead C skewing the mean age (Sierra *et al.*, 2018). However, inputs of ^{14}C-dead OC_{petro} are not considered in He *et al.* (2016) and Shi *et al.* (2020), despite the recognition that OC_{petro} inputs result in an "apparent" ageing of soil OC_{bio}.

Here, we quantify OC_{petro} in globally distributed soil profiles using the International Soil Radiocarbon Database (ISRaD database, see Supplementary Information) (Lawrence *et al.*, 2020). We separate soil profiles developed on igneous rocks (IG: negligible OC_{petro}) *versus* sedimentary rocks (SED: potential OC_{petro} inputs) using global geological maps and compare bulk ^{14}C signatures and % OC distributions. Alongside the global data set, using a mixing model analysis, we compare measurements made on river and soil OC in settings where OC_{petro} inputs have been demonstrated and where OC_{petro} is absent. Together, we assess the contribution of OC_{petro} to deep soils around the world and the implications for soil radiocarbon inventories and the surface carbon cycle.

1. Department of Geography, Durham University, South Road, Durham, DH1 3LE, UK
2. Center for Accelerator Mass Spectrometry, Lawrence Livermore National Laboratory, 7000 East Ave, Livermore, CA 94550, USA
3. Department of Earth Sciences, University of Oxford, South Parks Rd, Oxford, OX1 3AN, UK
4. Department of Marine Chemistry and Geochemistry, Woods Hole Oceanographic Institution, 266 Woods Hole Road, Woods Hole, MA 02543, USA
* Corresponding author (email: grant39@llnl.gov)

Evidence of OC_{petro} in soils and rivers using mixing models

The ^{14}C-depletion of soil OC can result from both: (1) ageing of OC_{bio} from plant and microbial derived material, stabilised by physical/chemical protection or intrinsic refractory properties (Hemingway *et al.*, 2019); and (2) mixing of OC_{petro} from rocks (^{14}C-free relative to instrumental background) with OC_{bio} (Petsch *et al.*, 2001; Hemingway *et al.*, 2018). To explore these scenarios, we examine cases where OC_{petro} contributes to bulk OC in river sediment loads and soils, with OC_{petro} inputs identified from geochemical proxies other than bulk ^{14}C (*e.g.*, C/N, $\delta^{13}C$, biomarkers, Raman spectroscopy, Ramped Pyrolysis Oxidation-^{14}C). These can be compared to examples where OC_{petro} inputs are absent and OC_{bio} decay/ageing acts alone from river sediments and soils on igneous bedrock (Fig. 1a, c). We find a notable contrast in the relationship between 1/[OC] and $\Delta^{14}C$ in sedimentary and igneous bedrock settings. Patterns expected for mixing between OC_{petro} and OC_{bio} appear to dominate in sedimentary settings.

An Andean Mountain river draining shales (Clark *et al.*, 2017) has river sediment OC $\Delta^{14}C$ values that ranged from −0.5 ‰ to −839 ‰. Clark *et al.* (2017) concluded that, on average, 0.37 ± 0.03 % of the suspended sediment mass was OC_{petro}. There is a significant linear trend between $\Delta^{14}C$ values and 1/[OC] ($p < 0.05$, $R^2 = 0.75$, Fig. 1a) that was attributed to binary mixing of OC_{petro} and biospheric OC supplied by erosion processes. In Himalayan rivers, the river OC also has a linear relationship between these variables ($p < 0.05$, $R^2 = 0.37$), albeit with a shallower slope due to lower OC_{petro} contents (Galy *et al.*, 2015). In soils, OC_{petro} has been recognised in only a few studies (Petsch, 2014; Hemingway *et al.*, 2018; Hilton *et al.*, 2021; Kalks *et al.*, 2021). In Taiwan, high erosion rates continuously supply fresh bedrock to the surface and keep surface soils young, and these samples have a linear relationship between $\Delta^{14}C$ and 1/[OC]. Mixing models show that OC_{petro} input to sediments and soils result in a linear trend between 1/[OC] and $\Delta^{14}C$ (Supplementary Information, Eq. S-8; Fig. 1b). These can explain the main patterns seen in the Andes and Himalayan rivers and Taiwanese soil data.

In contrast to the river sediments draining sedimentary rocks, rivers from a basaltic catchment, the Efri Haukadalsá River in Iceland (Torres *et al.*, 2020), have ^{14}C value ranging from −60 ‰ to −395 ‰ and display no relationship between 1/[OC] and $\Delta^{14}C$ (Fig. 1c). Torres *et al.* (2020) attributed the ^{14}C-depletion to erosion of millennial-aged OC from soils. In tropical soils, formed along a climate gradient underlain by a 450 ka lava flow from Hawaii, [OC] remains high while OC ages due to Fe-oxide mineral-carbon stabilisation, and these materials have an almost vertical array in 1/[OC] and $\Delta^{14}C$ (Fig. 1c; Grant *et al.*, 2022). These patterns in the data are more consistent with the paired evolution of 1/[OC] and $\Delta^{14}C$ expected for OC loss and ageing of OC, explored here using a simple organic matter degradation model (Supplementary Information sections 4.1 and 4.2).

Overall, the river and soil data here show how 1/[OC] and $\Delta^{14}C$ can be used to examine the role of OC_{petro} input. A domain of OC and $\Delta^{14}C$ values can most easily be reached by OC_{petro} addition to the organic matter pool (Fig. 1b), as seen in the grey "mixing zone" of sedimentary soils. In the igneous soils, this mixing domain is harder to populate. We note the importance of OC_{petro} is likely to be most relevant in soils with low OC_{bio} inputs or relatively old ^{14}C mean ages, which could be particularly important in deep soils (Rumpel and Kögel-Knabner, 2011; Shi *et al.*, 2020).

Widespread OC_{petro} input to global soils

To assess a potential, wider input of OC_{petro} into soils, we use the ISRaD database (Lawrence *et al.*, 2020) (see Supplementary Information). All database samples used have reported $\Delta^{14}C$ values and *measured* (not extrapolated or modelled) [OC] (Fig. 2a). We characterise the parent material for each geo-located profile from the global lithological map database (GLiM) (Hartmann and Moosdorf, 2012) if no parent material is specified in the database (79.4 % of entries). The soil radiocarbon profiles are split into sedimentary (SED) (80.9 %) and igneous (IG) (19.4 %) parent material, with 557 soil profiles and 2978 radiocarbon measurements (Supplementary Information) (Fig. 2e). There are more SED profiles (397 profiles, 2260 measurements) than IG profiles (160 profiles, 718 measurements), broadly mirroring the fact that ~60 % of Earth's terrestrial surface is composed of sedimentary rock (Hartmann and Moosdorf, 2012). An important caveat is that we do not capture all Quaternary deposits such

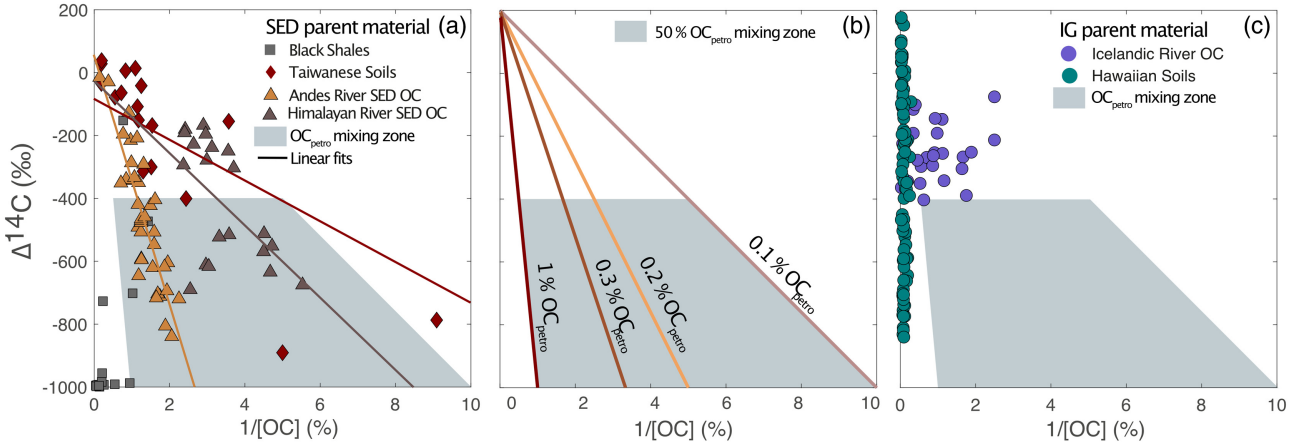

Figure 1 Rock organic carbon imprints on organic carbon concentration (OC) and radiocarbon activity ($\Delta^{14}C$). **(a)** Samples from Taiwanese soils, Andes and Himalayan rivers, and black shale weathering profiles where OC_{petro} inputs are known, with linear fits through data shown. **(b)** Binary mixing model (lines) between OC_{bio} ($\Delta^{14}C = +200$ ‰) and OC_{petro} (varying from 1 % to 0.1 % of total OC, $\Delta^{14}C = -1000$ ‰). The grey shaded area is where >50 % of total OC is OC_{petro}. **(c)** Samples where OC_{petro} is absent: soil from Hawaiian Pololu lava flow and Icelandic river samples draining basalt.

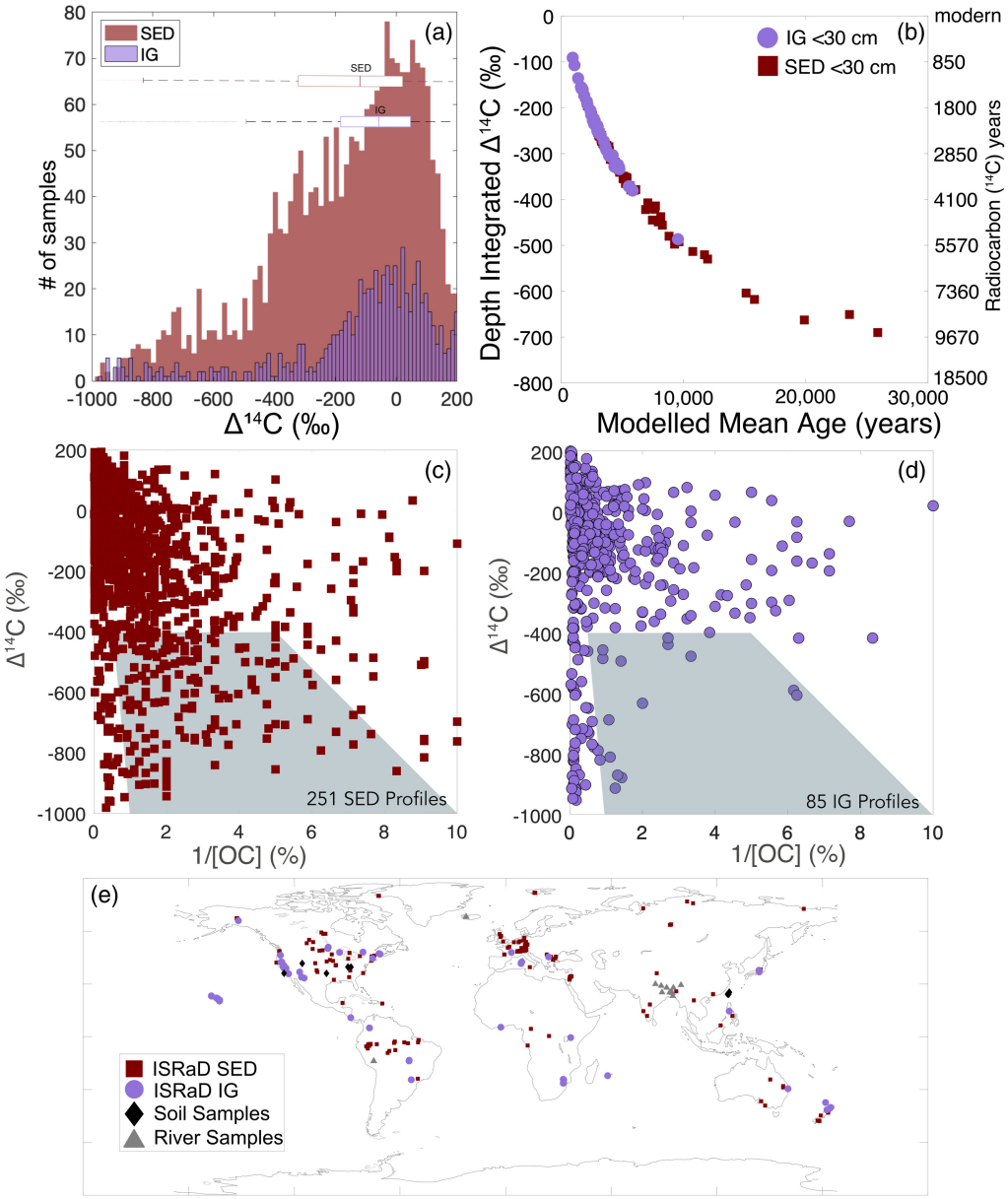

Figure 2 **(a)** The distribution of radiocarbon measurements for the SED and IG profiles, with corresponding box plots depicting the median and quartiles of the distributions. **(b)** The depth integrated $\Delta^{14}C$ (displayed in ‰ and ^{14}C years) *vs.* modelled mean ages extracted from the Shi *et al.* (2020) dataset for the SED and IG profiles. **(c)** The ISRaD soil horizons from SED soils plotted in 1/[OC] and radiocarbon ($\Delta^{14}C$). **(d)** The ISRaD soil horizons from IG soils plotted in 1/[OC] and radiocarbon activity ($\Delta^{14}C$). The grey shaded region defines a zone where mixing of OC_{petro} can produce compositions which are difficult to obtain via OC decomposition alone (Fig. 1b). **(e)** Locations of samples where direct measurement of OC_{petro} inputs have been identified (diamond, triangle), and soil profiles from the ISRaD database on igneous (IG, circles) and sedimentary rocks (SED, squares).

as loess or ashfall, which are important parent materials for soil (Baisden and Parfitt, 2007). Rather than filter the database further, we note some of the SED samples on loess or ashfall may have very low OC_{petro} inputs.

Despite the complexities inherent in any global soil assessment (Lawrence *et al.*, 2020), characterising samples from ISRaD as from either SED or IG sites reveals patterns which can be accounted for by OC_{petro} inputs. First, the median and lower quartile $\Delta^{14}C$ values of SED samples are lower than IG sites (Fig. 2c, Table S-2). Second, the distribution of SED and IG soil $\Delta^{14}C$ values are significantly different at the 0.05 level (Kolomogorov-Smirnov Test). Third, the calculated profile-averaged $\Delta^{14}C$ values and modelled mean soil age are significantly different between SED and IG profiles ($p > 0.05$, Supplementary Information section 1.3). Finally, the SED samples that reach lower $\Delta^{14}C$ values (Fig. 2c) define the grey zone suggested by a binary mixing model (Fig. 1b). IG profiles do not commonly reach this range of compositions, with the ^{14}C depleted samples either having retained higher % OC, or remain fairly ^{14}C-enriched ($\Delta^{14}C > -200$ ‰) as OC is lost, *i.e.* have a shallower trajectory between 1/[OC] and $\Delta^{14}C$ (Fig. 2d).

Having established potential OC_{petro} inputs at SED sites, the radiocarbon data can be used to quantify a maximum permissible OC_{petro} input. To do so, we assume all ^{14}C-depletion is driven by OC_{petro} addition (*i.e.* no OC_{bio} ageing) (Supplementary Information section 5.1). We calculate an average maximum proportion of $OC_{petro} = 0.38$ or 38 % (Fig. 3b) for all SED soils. This corresponds to an average 0.85 ± 0.1 % OC_{petro} in soils (Fig. 3c).

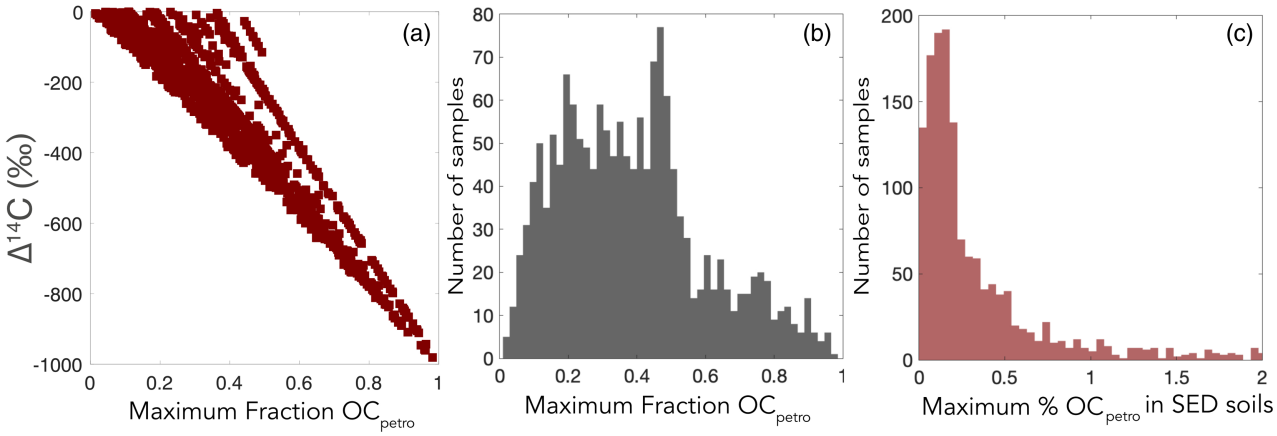

Figure 3 **(a)** The maximum fraction of [OC_{petro}] is calculated via a binary mixing model between OC_{bio} and OC_{petro} in the globally distributed soil profiles (ISRaD database). **(b)** A histogram of the maximum fraction of OC_{petro} values for each soil sample. The mean f_{petro} is 0.38 ± 0.01, the median value is 0.36. **(c)** A histogram of calculated maximum OC_{petro} (wt. %) in each SED soil horizon. The average is 0.85 ± 0.1 wt. % OC and the median is 0.19 % OC_{petro} in SED soils globally.

This maximum value is reasonable given known OC contents of sedimentary rocks (Graz *et al.*, 2011; Partin *et al.*, 2013).

Taken together, our analysis places a maximum bound on the OC_{petro} content to deep and ^{14}C depleted soils forming on sedimentary rocks. While this estimation is an upper bound because OC_{bio} ageing will occur in deep soils (Grant *et al.*, 2022), and does not consider loss of OC_{petro} during weathering, it is a reasonable starting point to understand how incorporation of OC_{petro} can influence mean soil age.

OC_{petro} in soils leads to mean age overestimation

Input of OC_{petro} in soils formed on sedimentary rocks is consistent with patterns in the dataset (Fig. 2c, d). If OC_{petro} contributes to deep soils, how much could it alter carbon residence times based on ^{14}C measurements? To provide a first constraint, we reconsider the Shi *et al.* (2020) global weighted $\Delta^{14}C$ accounting for a fraction of OC_{petro}. The mean age in subsoils (30–100 cm depth) was $\Delta^{14}C = -391 \pm 56$ ‰ (~3970 ^{14}C years). Accounting for our calculated maximum fraction of 0.38 OC_{petro} could mean the OC_{bio} age calculated in the Shi *et al.* (2020) dataset is equivalent to −17.7 ‰, or 150 ^{14}C years, a difference of ~3800 ^{14}C years. Using a more modest mass fraction of 0.10 for OC_{petro} would shift the biospheric radiocarbon age younger by 800 ^{14}C years (from 3900 to 3100 ^{14}C yr). While a 38 % OC_{petro} contribution is likely an overestimation, the analysis shows that even modest OC_{petro} inputs could shift assessments of OC_{bio} residence time in soils, yet OC_{petro} inputs are not considered in global assessments (He *et al.*, 2016; Shi *et al.*, 2020). An "apparent" increase in OC_{bio} age by failing to account for OC_{petro} addition would imply soil carbon exchange fluxes with the atmosphere are underestimated. Accounting for the fate of OC_{petro} in soils is important for reducing uncertainty on the present and future role of soils in the anthropogenic carbon budget.

The input of OC_{petro} to soils is central to the long-term carbon cycle. It is important to assess the OC_{petro} input to soils, its oxidation during soil formation that can release CO_2, and the potential influence of OC_{petro} on soil OC stabilisation mechanisms. We can compare our maximum OC_{petro} contents (Fig. 3) from the SED soil profiles from ISRaD to global sedimentary rock OC values (Fig. S-3). These sedimentary rock samples have higher OC contents than sedimentary soils, suggesting the widespread loss of OC_{petro} in global soils (Partin *et al.*, 2013). Traditionally, OC_{petro} is considered inert or unreactive on anthropogenic timescales. However, in Taiwanese soils, Hemingway *et al.* (2018) found that ~67 % of OC_{petro} was lost during soil formation, even during rapid erosion which limits time for soil weathering. This extensive OC_{petro} oxidation was attributed to microbial assimilation of OC_{petro} (Hemingway *et al.*, 2018). To move forward, we must recognise that, like OC_{bio} in soil, OC_{petro} is a continuum of compounds which differ in chemistry, linked to the history of past sedimentation, diagenesis, and metamorphism (Galy *et al.*, 2008; Petsch, 2014) which may have a distribution of reactivities and residence times in soils. Radiocarbon measurements suggest that OC_{petro} contribution to soils is a global feature and so needs to be considered to properly constrain soil carbon storage and turnover. Quantifying the fate of OC_{petro} in soils is then crucial to understanding the evolution of the long-term carbon and oxygen cycles.

Acknowledgements

This work was performed under the European Research Council (ERC) Starting Grant (678779, ROC-CO_2) and partly under an ERC Consolidator Grant (101002563, RIV-ESCAPE) to RGH. Partial writing of this work was performed under the auspices of the U.S. Department of Energy by Lawrence Livermore National Laboratory under contract DE-AC52-07NA27344 (LLNL-JRNL-837045).

Editor: Liane G. Benning

Additional Information

Supplementary Information accompanies this letter at https://www.geochemicalperspectivesletters.org/article2312.

Cite this letter as: Grant, K.E., Hilton, R.G., Galy, V.V. (2023) Global patterns of radiocarbon depletion in subsoil linked to rock-derived organic carbon. *Geochem. Persp. Let.* 25, 36–40. https://doi.org/10.7185/geochemlet.2312

References

Agnelli, A., Trumbore, S.E., Corti, G., Ugolini, F.C. (2002) The dynamics of organic matter in rock fragments in soil investigated by ^{14}C dating and measurements of ^{13}C. *European Journal of Soil Science* 53, 147–159. https://doi.org/10.1046/j.1365-2389.2002.00432.x

Baisden, W.T., Parfitt, R.L. (2007) Bomb ^{14}C enrichment indicates decadal C pool in deep soil? *Biogeochemistry* 85, 59–68. https://doi.org/10.1007/s10533-007-9101-7

Clark, K.E., Hilton, R.G., West, A.J., Robles Caceres, A., Gröcke, D.R., Marthews, T.R., Ferguson, R.I., Asner, G.P., New, M., Malhi, Y. (2017) Erosion of organic carbon from the Andes and its effects on ecosystem carbon dioxide balance. *Journal of Geophysical Research: Biogeosciences* 122, 449–469. https://doi.org/10.1002/2016JG003615

Copard, Y., Amiotte-Suchet, P., Di-Giovanni, C. (2007) Storage and release of fossil organic carbon related to weathering of sedimentary rocks. *Earth and Planetary Science Letters* 258, 345–357. https://doi.org/10.1016/j.epsl.2007.03.048

Galy, V., Beyssac, O., France-Lanord, C., Eglinton, T. (2008) Recycling of Graphite During Himalayan Erosion: A Geological Stabilization of Carbon in the Crust. *Science* 322, 943–945. https://doi.org/10.1126/science.1161408

Galy, V., Peucker-Ehrenbrink, B., Eglinton, T. (2015) Global carbon export from the terrestrial biosphere controlled by erosion. *Nature* 521, 204–207. https://doi.org/10.1038/nature14400

Grant, K.E., Galy, V.V., Haghipour, N., Eglinton, T.I., Derry, L.A. (2022) Persistence of old soil carbon under changing climate: The role of mineral-organic matter interactions. *Chemical Geology* 587, 120629. https://doi.org/10.1016/j.chemgeo.2021.120629

Graz, Y., Di-Giovanni, C., Copard, Y., Elie, M., Faure, P., Laggoun Defarge, F., Lévèque, J., Michels, R., Olivier, J.E. (2011) Occurrence of fossil organic matter in modern environments: Optical, geochemical and isotopic evidence. *Applied Geochemistry* 26, 1302–1314. https://doi.org/10.1016/j.apgeochem.2011.05.004

Hartmann, J., Moosdorf, N. (2012) The new global lithological map database GLiM: A representation of rock properties at the Earth surface. *Geochemistry, Geophysics, Geosystems* 13, Q12004. https://doi.org/10.1029/2012GC004370

He, Y., Trumbore, S.E., Torn, M.S., Harden, J.W., Vaughn, L.J.S., Allison, S.D., Randerson, J.T. (2016) Radiocarbon constraints imply reduced carbon uptake by soils during the 21st century. *Science* 353, 1419–1424. https://doi.org/10.1126/science.aad4273

Hemingway, J.D., Hilton, R.G., Hovius, N., Eglinton, T.I., Haghipour, N., Wacker, L., Chen, M.-C., Galy, V.V. (2018) Microbial oxidation of lithospheric organic carbon in rapidly eroding tropical mountain soils. *Science* 360, 209–212. https://doi.org/10.1126/science.aao6463

Hemingway, J.D., Rothman, D.H., Grant, K.E., Rosengard, S.Z., Eglinton, T.I., Derry, L.A., Galy, V.V. (2019) Mineral protection regulates long-term global preservation of natural organic carbon. *Nature* 570, 228–231. https://doi.org/10.1038/s41586-019-1280-6

Hilton, R.G., West, A.J. (2020) Mountains, erosion and the carbon cycle. *Nature Reviews Earth & Environment* 1, 284–299. https://doi.org/10.1038/s43017-020-0058-6

Hilton, R.G., Turowski, J.M., Winnick, M., Dellinger, M., Schleppi, P., Williams, K.H., Lawrence, C.R., Maher, K., West, M., Hayton, A. (2021) Concentration-Discharge Relationships of Dissolved Rhenium in Alpine Catchments Reveal Its Use as a Tracer of Oxidative Weathering. *Water Resources Research* 57, e2021WR029844. https://doi.org/10.1029/2021WR029844

Jackson, R.B., Lajtha, K., Crow, S.E., Hugelius, G., Kramer, M.G., Piñeiro, G. (2017) The Ecology of Soil Carbon: Pools, Vulnerabilities, and Biotic and Abiotic Controls. *Annual Review of Ecology, Evolution, and Systematics* 48, 419–445. https://doi.org/10.1146/annurev-ecolsys-112414-054234

Kalks, F., Noren, G., Mueller, C.W., Helfrich, M., Rethemeyer, J., Don, A. (2021) Geogenic organic carbon in terrestrial sediments and its contribution to total soil carbon. *Soil* 7, 347–362. https://doi.org/10.5194/soil-7-347-2021

Lawrence, C.R., Beem-Miller, J., Hoyt, A.M., Monroe, G., Sierra, C.A., *et al.* (2020) An open-source database for the synthesis of soil radiocarbon data: International Soil Radiocarbon Database (ISRaD) version 1.0. *Earth System Science Data* 12, 61–76. https://doi.org/10.5194/essd-12-61-2020

Mathieu, J.A., Hatté, C., Balesdent, J., Parent, É. (2015) Deep soil carbon dynamics are driven more by soil type than by climate: a worldwide meta-analysis of radiocarbon profiles. *Global Change Biology* 21, 4278–4292. https://doi.org/10.1111/gcb.13012

Partin, C.A., Bekker, A., Planavsky, N.J., Scott, C.T., Gill, B.C., Li, C., Podkovyrov, V., Maslov, A., Konhauser, K.O., Lalonde, S.V., Love, G.D., Poulton, S.W., Lyons, T.W. (2013) Large-scale fluctuations in Precambrian atmospheric and oceanic oxygen levels from the record of U in shales. *Earth and Planetary Science Letters* 369–370, 284–293. https://doi.org/10.1016/j.epsl.2013.03.031

Petsch, S.T. (2014) 12.8 - Weathering of Organic Carbon. In: Holland, H.D., Turekian, K.K. (Eds.) *Treatise on Geochemistry*. Second Edition, Elsevier, Amsterdam, 217–238. https://doi.org/10.1016/B978-0-08-095975-7.01013-5

Petsch, S.T., Eglinton, T.I., Edwards, K.J. (2001) ^{14}C-Dead Living Biomass: Evidence for Microbial Assimilation of Ancient Organic Carbon During Shale Weathering. *Science* 292, 1127–1131. https://doi.org/10.1126/science.1058332

Rumpel, C., Kögel-Knabner, I. (2011) Deep soil organic matter—a key but poorly understood component of terrestrial C cycle. *Plant and Soil* 338, 143–158. https://doi.org/10.1007/s11104-010-0391-5

Schmidt, M.W.I., Torn, M.S., Abiven, S., Dittmar, T., Guggenberger, G., Janssens, I.A., Kleber, M., Kögel-Knabner, I., Lehmann, J., Manning, D.A.C., Nannipieri, P., Rasse, D.P., Weiner, S., Trumbore, S.E. (2011) Persistence of soil organic matter as an ecosystem property. *Nature* 478, 49–56. https://doi.org/10.1038/nature10386

Shi, Z., Allison, S.D., He, Y., Levine, P.A., Hoyt, A.M., Beem-Miller, J., Zhu, Q., Wieder, W.R., Trumbore, S., Randerson, J.T. (2020) The age distribution of global soil carbon inferred from radiocarbon measurements. *Nature Geoscience* 13, 555–559. https://doi.org/10.1038/s41561-020-0596-z

Sierra, C.A., Hoyt, A.M., He, Y., Trumbore, S.E. (2018) Soil Organic Matter Persistence as a Stochastic Process: Age and Transit Time Distributions of Carbon in Soils. *Global Biogeochemical Cycles* 32, 1574–1588. https://doi.org/10.1029/2018GB005950

Torres, M.A., Kemeny, P.C., Lamb, M.P., Cole, T.L., Fischer, W.W. (2020) Long-Term Storage and Age-Biased Export of Fluvial Organic Carbon: Field Evidence From West Iceland. *Geochemistry, Geophysics, Geosystems* 21, e2019GC008632. https://doi.org/10.1029/2019GC008632

Trumbore, S. (2000) Age of Soil Organic Matter and Soil Respiration: Radiocarbon Constraints on Belowground C Dynamics. *Ecological Applications* 10, 399–411. https://doi.org/10.1890/1051-0761(2000)010[0399:AOSOMA]2.0.CO;2

Geochemical Perspectives Letters

Global patterns of radiocarbon depletion in subsoil linked to rock-derived organic carbon

K.E. Grant, R.G. Hilton, V.V. Galy

Supplementary Information

The Supplementary Information includes:

1. ISRaD Database Screening and Geological Maps

1.1 Database parent material. We used the ISRaD database (ISRaD_data_v1.3.4.2020) of soil radiocarbon measurements (reported as $\Delta^{14}C$) to explore the role of rock organic carbon (OC_{petro}) inputs. Over 79 % of the soils listed in the ISRaD database do not have parent material information or chemistry. Table S-1 shows all listed parent material variables in the ISRaD database, with the number of entries, relative proportion of entries, and final designation we assigned using external geological mapping (see section 1.2). Of the data fields listed in the ISRaD database (a total of 181) we used the 'lyr_c_org', 'lyr_c_tot', 'lyr_14c', 'lyr_fraction_modern', 'pro_name', 'pro_parent_material', 'pro_treatment', 'site_lat', and 'site_long' for this analysis. Other data fields were not used in this study.

Table S-1 Parent Material Categories listed in ISRaD database.

ISRaD Parent Material Designation	# of entries	Proportion of total (%)	GLiM Designation
'NA'	13,842	79.4	assigned
'evaporites'	59	0.3	removed
'igneous extrusive'	163	0.9	IG
'igneous intrusive'	630	3.6	IG
'igneous pyroclastic'	229	1.3	IG
'interbedded'	13	0.1	SED
'loess'	465	2.7	removed
'metamorphic'	379	2.2	SED
'organic'	283	1.6	removed
'sedimentary-clastic'	1361	7.8	SED
Total	17,424		

1.2 Assessment of bedrock geology at ISRaD soil profile locations. To assign generalised parent material for each sample in the ISRaD database we used the site location (latitude and longitude) and compared that location to the bedrock geology of the global lithologic map (GLiM) (Hartmann and Moosdorf, 2012). The GliM is a GIS layer of bedrock or exposed surface rock on the Earth in a 0.5 by 0.5 degree grid space. It is the highest resolution grid for a global surface land model for rock type. The GliM has 16 simplified lithologic classes of parent material or exposed surface rock. We collated these rock types to form the SED and IG definitions. For the purposes here, we use only these primary lithologic classes, rather than the subclasses, and as such this approach simplifies the heterogeneity that can exist within potential sedimentary rock types.

For samples with parent material field reported with 'NA' in the ISRaD database (13,842) we assign a designation of SED or IG based on the co-located bedrock from the GLiM database. For the SED designation, we used five classes (mt: Metamorphic, sc: Carbonate sedimentary rocks, sm: Mixed sedimentary rocks, ss: Siliciclastic sedimentary rocks, su: Unconsolidated sediments) and for the IG we used pa: Acid plutonic rocks, pb: Basic plutonic rocks, pi: Intermediate plutonic rocks, py: pyroclastic, va: Acid volcanic rocks, vi: intermediate volcanic rocks. Excluded from both the sedimentary and igneous datasets were profiles that were designated as on the ic: Ice and glaciers and on wb: waterbodies by the GLiM database. Additionally, any sites that had listed parent material in ISRaD categorised as follows 'interbedded', 'sedimentary-clastic', and 'metamorphic' as SED, while 'igneous extrusive', igneous intrusive', igneous pyroclastic' are designated as IG. The other parent material designations of 'evaporates', 'loess', and 'organic' were removed from this analysis. Additionally, in both the SED or IG designations the 'treatment' profiles were removed. Hereafter, any soil profile with sedimentary parent material is designated (SED) (397 profiles; 2260 individual entries) and soil profiles formed on igneous parent material are (IG) (160 profiles; 718 entries). We used a total of 557 profiles in the study, with 2978 total horizons.

1.3 Globally modelled mean age and $\Delta^{14}C$. To assign the modelled mean age and depth integrated $\Delta^{14}C$ at each of our SED or IG profile locations, we use spatially resolved global datasets of soil OC mean age and depth integrated $\Delta^{14}C$ published by Shi *et al*. (2020). Using locations of each of our previously designated SED and IG profiles, we extract the depth resolved $\Delta^{14}C$ values and modelled mean ages at each of the 397

SED and 160 IG profiles. We find that the distributions of the both the mean age and the depth resolved $\Delta^{14}C$ for our designated SED and IG profiles are statistically different using a Kruskal Wallis test for both the subsoils (<30 cm) and the entire averaged profile ($p > 0.05$). This could be explained by a previously unaccounted for input of OC_{petro} in the SED profiles.

2. Summary of Radiocarbon ($\Delta^{14}C$) Data from ISRaD Soil Profiles

2.1 ISRaD radiocarbon summary. For the radiocarbon data, the ISRaD database contains entries reported in either fraction modern (Fm) and $\Delta^{14}C$ values. Any entry as Fm was converted to $\Delta^{14}C$ using Eq. S-1 and the sampling year reported in the database:

$$\Delta^{14}C = \left[Fm * e^{\lambda(1950-Y_c)} - 1\right] \times 1000 \quad \text{(S-1)}$$

where Y_c is the sampling year listed in the database (pro_year). Table S-2 shows the summary statistics for the entire $\Delta^{14}C$ database. The $\Delta^{14}C$ depth profiles for each soil profile show radiocarbon depletion is strongly linked with depth (Fig. S-2) as has been seen in other studies (Mathieu *et al.*, 2015; He *et al.*, 2016; Shi *et al.*, 2020).

Table S-2 Radiocarbon signatures ($\Delta^{14}C$) and % OC for SED and IG.

	Total Dataset $\Delta^{14}C$		Total Dataset (% OC)	
	SED	IG	SED	IG
# samples	2260	718	2260	718
% of total	100	100	100	100
mean	−164.6	−115.2	7.3	8.0
standard deviation (±s.d.)	259.1	261.1	14.5	11.8
standard error (±s.e.)	5.5	9.7	0.30	0.44
median	−112.9	−49.9	1.0	2.5
minimum	−981.0	−976.5	0.0	0.0
maximum	675.2	278.8	92.8	55.0

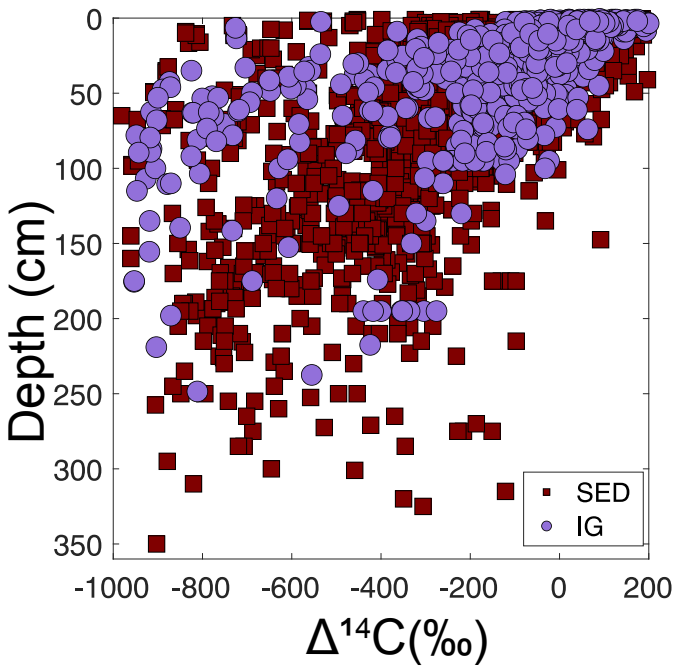

Figure S-1 The radiocarbon activity ($\Delta^{14}C$) of ISRaD soil samples plotted as a function of depth.

3. Measured Soil and River Samples with Known OC_{petro} Inputs

We use soil samples and river sediment and suspended particulate samples where OC_{petro} incorporation was identified using other geochemical measurements. We use a mixture of soil profiles and river samples for two reasons. Firstly, there have been very few studies to look at OC_{petro} evolution and influence within individual soil profiles. Secondly, we use rivers to understand the catchment wide influence of bedrock influence on the sampling of river OC.

3.1 River inputs of OC_{petro}. The two river systems, Andean and Himalayan, draining sedimentary rock basins have been extensively studied, so we have a reasonable understanding of OC_{petro} input to these rivers. For Andean river OC, evolution of N/C and $\delta^{13}C$ strongly suggests mixing of OC from soils and bedrocks, which were independently sampled. This mixing of OC_{petro} and OC_{bio} was confirmed by ^{14}C measurements (Clark *et al.*, 2013, 2017). For Himalayan river OC, Galy *et al.* (2008) used Raman spectroscopy to identify recycled graphite reaching rivers. This conclusively demonstrated that OC_{petro} was incorporated into the 'modern' river system through weathering. In another study, ramped pyrolysis/oxidation (RPO-^{14}C) coupled to ^{14}C measurements was used to identify a high temperature, ^{14}C 'dead' component in the river OC. This technique was used to quantify the rock OC input to the river system (Rosenheim and Galy, 2012).

3.2 Soil inputs of OC_{petro}. For soil samples, a study done in Taiwan was chosen based on its conclusive examination of OC_{petro} occurrence during soil paedogenesis, erosion, and weathering. Taiwan soil OC which has been studied extensively using both RPO-^{14}C and lipid biomarkers (abundance, ^{13}C, and ^{14}C isotope composition) to trace OC_{petro} though a soil weathering profiles, and ultimately record OC_{petro} oxidation in rapidly eroding soils (Hemingway *et al.*, 2018).

While we also consider black shale weathering profiles as soil, they are more accurately described as an oxidative weathering profile. They are formed by weathering rather than a "top down" soil forming process. These well studied samples reflect a high [OC] with completely depleted ^{14}C signature and are a specific case endmember to show OC_{petro} can be lost in a profile (Petsch *et al.*, 2001).

4. Model Expectations

4.1. Soil decay model. To explore the range of OC and $\Delta^{14}C$ values expected for organic matter undergoing decay in soil, we model loss of OC (lowering [OC], %) as the material ages and the loss of ^{14}C by radioactive decay (Eq. S-1). Radiocarbon is continually produced in the atmosphere and is incorporated into the biosphere through photosynthesis. Soils become enriched in ^{14}C *via* plant inputs. Subsequently, this organic matter can be distributed into multiple soil reservoirs, which can be modelled numerically as individual "pools" (Eq. S-2) in the soil with different residence time. These can reflect different depths in a soil, and/or different physical and/or bio-chemical characteristics which alter the degradation of organic matter:

$$C(t) = \sum_{i=1-3}^{n} C_i(t) \tag{S-2}$$

where C is the total OC remaining through time and is a function of 1 to 3 different pools (i) with different residence times. Soil OC decay models with 1, 2 or 3 pools, each with different OC decay constants, k_i were explored. We assume a steady state system and are therefore only interested in the decay or output of the "box", so we can explicitly solve for the change in the soil decay as:

$$\frac{dC_{\mathrm{Tot}}}{dt} = -k_i \times C_i(t) \tag{S-3}$$

The metric $1/k_i$ is commonly referred to as the turnover time (Sierra *et al.*, 2017). The model is not trying to fit the data, but instead track the range of expected values of 1/OC and $\Delta^{14}C$. As such, we do not make the model more complex by considering interacting pools (Schuur *et al.*, 2016) and start with [OC] = 30 % (Fig. S-2), representing plant organic matter inputs, and then follow the trajectory with no additional OC input. These models track the loss of OC over a fixed amount of time. All modelling was done using Matlab version R2019b.

We tested parallel multiple pool models (2 and 3 pools) with turnover times representing "fast", "slow", and "inert" OC decay. A "multi-pool" model may better describe a 'real' soil system (Gaudinski *et al.*, 2000; Manzoni *et al.*, 2009). In each model, we find that the low [OC] outputs, (*i.e.* [OC] < 1 %) are defined by the pool with the longest turnover time. So, for our study, a 1 pool model was representative of the average decay over long timescales and low total OC outputs, which are most relevant for assessing OC_{petro} input in deeper soil. We do not seek to unravel the complexity of rapid decay on shorter time scales. The soil decay model predicts non-linear trajectories in 1/[OC] versus $\Delta^{14}C$, with a steep drop and an asymptotic behaviour for a given turnover time (Fig. 1b).

4.2 Endmember mixing model. To explore the $\Delta^{14}C$ and [OC] values produced by mixing OC_{petro} and OC_{bio}, we use binary mixing models to calculate a range of OC_{petro} inputs. A two-endmember mixing model describing these two endmembers is defined as follows:

$$\Delta^{14}C_{mix} = f_{petro} \times \Delta^{14}C_{petro} + f_{bio} \times \Delta^{14}C_{bio} \quad \text{(S-4)}$$

$$1 = f_{petro} + f_{bio} \quad \text{(S-5)}$$

$$\%\ OC_{mix} = \%\ OC_{petro} + \%\ OC_{bio} \quad \text{(S-6)}$$

$$1 = \frac{\%\ OC_{petro}}{\%\ OC_{mix}} + \frac{\%\ OC_{bio}}{\%\ OC_{mix}} \quad \text{(S-7)}$$

$$\Delta^{14}C_{mix} = \frac{\%\ OC_{petro}}{\%\ OC_{mix}} \times \Delta^{14}C_{petro} + \frac{\%\ OC_{mix} - \%\ OC_{petro}}{\%\ OC_{mix}} \times \Delta^{14}C_{bio} \quad \text{(S-8)}$$

where Equation S-4 states that the bulk $\Delta^{14}C$ value of the sampled soil ($\Delta^{14}C_{mix}$) is a function of the fraction of OC_{petro} (f_{petro}) which by definition has $\Delta^{14}C_{petro} = -1000$ ‰ and the fraction of OC_{bio} (f_{bio}) with an $\Delta^{14}C_{bio}$ close to the atmospheric value. This OC_{bio} value is variable and based on the 'modern' input of OC to the soil, in this case $\Delta^{14}C_{bio}$ is typically >−100 ‰. In this instance all the organic carbon in the single soil sample is either petrogenic or biospheric (Eq. S-5), so the fraction of each must equal 1. This can be rewritten to reflect the known % OC measurements where the total sample % OC value is % OC_{mix} and the either measured or model % OC_{petro} and % OC_{bio} contributing to the % OC_{mix} (Eq. S-6). We can then substitute our Equation S-7 into Equation S-4 to solve for OC_{petro} (Eq. S-8) because we know the measured OC_{mix} and the bulk $\Delta^{14}C_{mix}$ and $\Delta^{14}C_{petro}$ and can estimate $\Delta^{14}C_{bio}$ from atmospheric values.

Here we consider the OC_{bio} endmember is $\Delta^{14}C = +200$ ‰ and the OC_{petro} endmember is, by definition, $\Delta^{14}C = -1000$ ‰. An aged OC_{bio} component is not considered here for simplicity, but if included it would bound the 'grey' region with a steeper slope and less area. The distinction in mixing of OC_{bio} with a 200 ‰ and 0 ‰ is only important at relatively young or enriched ^{14}C values. We consider OC_{petro} concentrations from 1 % to 0.1 %, and ^{14}C depletion below $\Delta^{14}C < -400$ ‰. This defines a mixing zone ("grey region") where OC_{petro} mixing can generate data in the 1/[OC] and $\Delta^{14}C$ space.

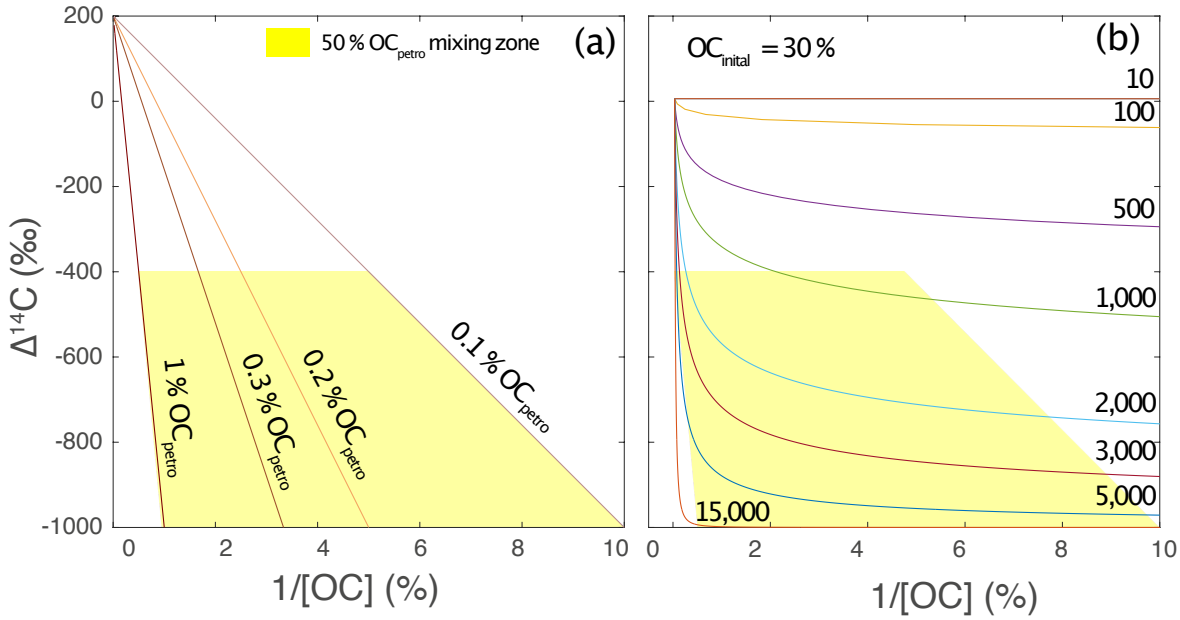

Figure S-2 **(a)** Binary mixing model (lines) between OC_{bio} ($\Delta^{14}C$ = +200 ‰) and OC_{petro} (varying from 1 % to 0.1 %, $\Delta^{14}C$ = −1000 ‰). The grey shaded area is where >50 % is OC_{petro}. B. **(b)** The predicted evolution of 1/[OC] and radiocarbon activity ($\Delta^{14}C$) for single pool OC decay models with turnover times (years) shown.

5. Maximum Permissible OC_{petro} Input to Soils

5.1 OC_{petro} in each horizon. Using the binary mixing model analysis described above (Eqs. S-2 to S-8) we calculate the maximum OC_{petro} input from rocks into each individual horizon using carbon concentration (% OC) and measured radiocarbon signature ($\Delta^{14}C$) of SED samples from the ISRaD database. We do this for samples that have radiocarbon values less than 0 ‰ because we assume values near modern would have little influence by OC_{petro} inputs. We solve Equation S-4 for the fraction of OC_{petro} that could be contributing to decrease the sample $\Delta^{14}C$, to the measured $\Delta^{14}C_{mix}$. We use a biospheric OC (OC_{bio}) $\Delta^{14}C$ value is determined by the average atmospheric $\Delta^{14}C$ value at the year reported in the ISRaD database. The atmospheric value is taken from Levin and Kromer (2004). Inclusion of an aged OC_{bio} endmember would lower the OC_{petro} contribution. We calculate a f_{petro} and OC_{petro} for each $\Delta^{14}C$ value <0 ‰ in our SED dataset (Table S-3). To provide a first constraint on this, we assume that OC_{bio} aging dominates the surface of SED soil profiles where $\Delta^{14}C$ > −200 ‰. For samples with $\Delta^{14}C$ < −200 ‰ (n = 877), the average % OC = 2.3 ± 0.3 and $\Delta^{14}C$ = −430 ± 6.4 ‰. If the OC_{petro} fraction was 0.38, *i.e.* ~38 % of the total OC (Fig. 3B), the residual OC_{bio} would have $\Delta^{14}C$ = −80.6 ‰.

Table S-3 Analysis of maximum % OC_{petro} input to SED samples.

	% OC_{petro}: $\Delta^{14}C \leq 0$ ‰	f_{petro}: $\Delta^{14}C \leq 0$ ‰
# samples	1565	1565
mean	0.85	0.38
standard deviation (±s.d.)	2.29	0.21
standard error (±s.e.)	0.06	0.01
median	0.19	0.36
minimum	0.0	0.0
maximum	22.5	1.0

5.2 Comparison to global sedimentary rocks. We compare maximum % OC_{petro} contribution calculated in the SED soil horizons to the known global distribution of OC in sedimentary rocks that has been previously published in Partin *et al.* (2013). We expect our calculated % OC_{petro} to be an overestimation in our soils, but compared to % OC in global sedimentary rocks, where by definition all OC is OC_{petro}, our average maximum calculated % OC_{petro} for soils is 6.5 times less than the average % OC in globally distributed sedimentary rocks. This is evidence for widespread oxidation of OC_{petro} during soil formation and weathering.

Table S-4 Global Sedimentary Rock % OC values taken from Partin *et al*. (2013).

	Total Dataset (% OC)	Zeros removed (% OC)	<20 % OC
# of samples	2730	2544	2451
mean	5.13	5.50	4.77
standard deviation (±s.d.)	6.34	6.41	5.18
standard error (±s.e.)	0.12	0.13	0.10
median	2.4	2.8	2.6
minimum	0	0.01	0.01
maximum	39.3	39.3	19.83

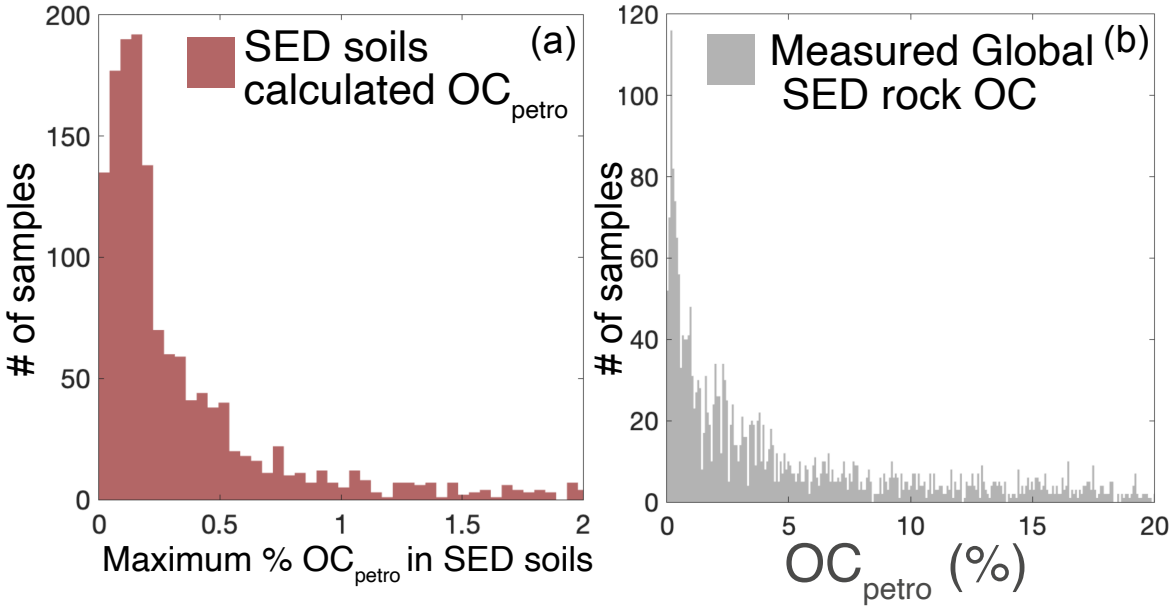

Figure S-3 **(a)** Calculated % OC_{petro} of the sedimentary parent material from the linear regression models from each SED soil profile. The data follows a general pattern of global sedimentary OC values. **(b)** Data extracted from Partin *et al*. (2013). Note the difference in the axis scales.

6. Caveats in the Global Approach

6.1 Preprocessing of soil samples: inorganic carbon removal. Our study requires the inclusion of samples with both *measured* total carbon and measured radiocarbon values. Total carbon was used in place of organic carbon values if organic carbon values were not reported. Most samples only reported total carbon measurements, without any specific information on the presence of inorganic carbon. In typical soil/sediment radiocarbon preparation, inorganic carbon (carbonate species) are removed prior to graphitisation *via* acid leaching or fumigation (Bao *et al.*, 2019). We assume that these published radiocarbon measurements would have undergone these pre-procedures if it was suspected detrital carbonates may be present, and thus that the dataset is not impacted by inorganic carbon inputs.

6.2 Preprocessing of soil samples: sieving. The standard protocol for soil profile sample collection includes the removal of rock fragments, either using a sieve or by hand (Soil Survey Staff, 2014). In this way, the ISRaD database may contain lower rock-derived inputs than is actually present in the environment. Nevertheless, sand, silt and clay materials in soils can still contain OC_{petro} (Agnelli *et al.*, 2002; Hemingway *et al.*, 2018; Kalks *et al.*, 2021). Rock fragments could be an important source of OC at all depths in a soil profile (Trumbore and Zheng, 1996; Agnelli *et al.*, 2002). It is traditional in soil studies to remove >2 mm fragments of the soil during sample processing before any geochemical analysis is completed. The >2 mm is reported by mass, but usually not measured otherwise. This practice may skew the radiocarbon age if those rock fragments have a measurable portion of OC derived from the parent material especially if the parent material contains OC_{petro}. The argument is that these particles are too large to play an active geochemical role, however this portion of the soil is actively weathering to create the <2 mm fraction. Most of the ISRaD database is likely to be comprised of measurement of the <2 mm portion of the soil, which would mean our assessment of OC_{petro} inputs is conservative in the SED profiles.

6.3 Presence of loess. We filtered the ISRaD database to remove profiles which mention Loess as the parent material (Table S-1). However, some of the N/A parent material classifications may be on loess, as this material is common in the USA Midwest and in East Asia. We have chosen not to actively filter further, recognising that loess material could contain rock OC, and it is a sedimentary structure, albeit not directly linked to the bedrock. The GLiM clearly states that it is measuring the parent material, likely exposed at the surface, but not the soil. As stated before, we have not used the subcategories for the GLiM due to simplicity. There is a chance that we would have a mixture of sources as the parent material as dust inputs, erosive material, or bedrock may be different than the exact surface exposure (Dere *et al.*, 2013). Therefore, in the very deep soils on "unconsolidated sediments" as is determined by the GLiM, as well as their secondary classification layer (lo: Loess), so while these sites may not be directly related to the "bedrock" the parent material in certainly sedimentary, and likely could contain 'rock' OC that has been weathered and transported.

6.4 Presence of clay minerals. The statistical differences in $\Delta^{14}C$ values for SED and IG samples support a role of OC_{petro} input. However, there could be other reasons that SED samples are more ^{14}C-depeleted, related to the presence of clay minerals. Mineral protection of OC can increase the relative proportion of ^{14}C-depleted OC in a sample. In volcanic, igneous basaltic soils, OC can be protected >10,000 years due to the short-range order mineral "gel" formed between co-precipitated OC and mineral matrix (Torn *et al.*, 1997). While this might suggest igneous parent material has a larger capacity to protect OC, thus resulting in more ^{14}C depleted OC, it is well established that more traditional clay minerals hosted in sedimentary rocks such as illite and kaolinite have a large capacity to sorb OC as well. These clay minerals can be formed as weathering products in granites, but are also common in sedimentary rocks, such as shales. Shales are formed through marine or lacustrine detrital sediment with high OC values during deposition. These clay minerals (both in size and minerology) can contribute to the stable OC content in shales, and this would suggest that shales can protect all types of OC through increased clay content (Basu *et al.*, 2019). It is reasonable that shale could protect even young carbon for extended periods of time. We cannot rule out a role of clay mineralogy and its difference between SED and IG profiles, and this represents an important topic for future work, the simpler explanation is that OC_{petro} inputs at SED sites explain the [OC] and $\Delta^{14}C$ distributions.

6.5 Implications of OC_{petro} input for SOC storage. OC_{petro} input could potentially alter SOC storage mechanisms in two ways. Generally, soil OC persistence mechanisms are either physical/chemical protection or intrinsic reactivity (Lehmann and Kleber, 2015). OC_{petro} is inherently part of the mineral fraction of the soil as it is a part of the bedrock. It likely will be both physically and chemically bonded to the mineral material. We hypothesise that the majority of the OC_{petro} would be in the heavy or mineral associated fraction, depending on the method used to fractionate or separate the soil pools (Lützow *et al.*, 2006). OC_{petro} in the mineral associated fraction would drive the measured radiocarbon age to be older while the actual age would be younger, just as we found in the bulk soils. In addition, OC_{petro} would be subject to oxidation as the surface area of the rock material is exposed to oxygen and water. Another hypothesis is this OC_{petro} could possibly contribute to additional sites for OC_{bio} accumulation due to organic-organic bonds (Possinger *et al.*, 2020) and contribute to additonal OC_{bio} storage. It is very diffucult to further comment on these processes without direct studies of the mineral bound soil carbon pool, and these remain avenues for future research.

Supplementary Information References

Agnelli, A., Trumbore, S.E., Corti, G., Ugolini, F.C. (2002) The dynamics of organic matter in rock fragments in soil investigated by ^{14}C dating and measurements of ^{13}C. *European Journal of Soil Science* 53, 147–159. https://doi.org/10.1046/j.1365-2389.2002.00432.x

Bao, R., McNichol, A.P., Hemingway, J.D., Lardie Gaylord, M.C., Eglinton, T.I. (2019) Influence of Different Acid Treatments on the Radiocarbon Content Spectrum of Sedimentary Organic Matter Determined by RPO/Accelerator Mass Spectrometry. *Radiocarbon* 61, 395–413. https://doi.org/10.1017/RDC.2018.125

Basu, S., Verchovsky, A.B., Bogush, A., Jones, A.P., Jourdan, A.-L. (2019) Stability of Organic Carbon Components in Shale: Implications for Carbon Cycle. *Frontiers in Earth Science* 7, 297. https://doi.org/10.3389/feart.2019.00297

Clark, K.E., Hilton, R.G., West, A.J., Malhi, Y., Gröcke, D.R., Bryant, C.L., Ascough, P.L., Robles Caceres, A., New, M. (2013) New views on "old" carbon in the Amazon River: Insight from the source of organic carbon eroded from the Peruvian Andes. *Geochemistry, Geophysics, Geosystems* 14, 1644–1659. https://doi.org/10.1002/ggge.20122

Clark, K.E., Hilton, R.G., West, A.J., Robles Caceres, A., Gröcke, D.R., Marthews, T.R., Ferguson, R.I., Asner, G.P., New, M., Malhi, Y. (2017) Erosion of organic carbon from the Andes and its effects on ecosystem carbon dioxide balance. *Journal of Geophysical Research: Biogeosciences* 122, 449–469. https://doi.org/10.1002/2016JG003615

Dere, A.L., White, T.S., April, R.H., Reynolds, B., Miller, T.E., Knapp, E.P., McKay, L.D., Brantley, S.L. (2013) Climate dependence of feldspar weathering in shale soils along a latitudinal gradient. *Geochimica et Cosmochimica Acta* 122, 101–126. https://doi.org/10.1016/j.gca.2013.08.001

Galy, V., Beyssac, O., France-Lanord, C., Eglinton, T. (2008) Recycling of Graphite During Himalayan Erosion: A Geological Stabilization of Carbon in the Crust. *Science* 322, 943–945. https://doi.org/10.1126/science.1161408

Gaudinski, J.B., Trumbore, S.E., Davidson, E.A., Zheng, S. (2000) Soil carbon cycling in a temperate forest: radiocarbon-based estimates of residence times, sequestration rates and partitioning of fluxes. *Biogeochemistry* 51, 33–69. https://doi.org/10.1023/A:1006301010014

Hartmann, J., Moosdorf, N. (2012) The new global lithological map database GLiM: A representation of rock properties at the Earth surface. *Geochemistry, Geophysics, Geosystems* 13, Q12004. https://doi.org/10.1029/2012GC004370

He, Y., Trumbore, S.E., Torn, M.S., Harden, J.W., Vaughn, L.J.S., Allison, S.D., Randerson, J.T. (2016) Radiocarbon constraints imply reduced carbon uptake by soils *during* the 21st century. *Science* 353, 1419–1424. https://doi.org/10.1126/science.aad4273

Hemingway, J.D., Hilton, R.G., Hovius, N., Eglinton, T.I., Haghipour, N., Wacker, L., Chen, M.-C., Galy, V.V. (2018) Microbial oxidation of lithospheric organic carbon in rapidly eroding tropical mountain soils. *Science* 360, 209–212. https://doi.org/10.1126/science.aao6463

Kalks, F., Noren, G., Mueller, C.W., Helfrich, M., Rethemeyer, J., Don, A. (2021) Geogenic organic carbon in terrestrial sediments and its contribution to total soil carbon. *Soil* 7, 347–362. https://doi.org/10.5194/soil-7-347-2021

Levin, I., Kromer, B. (2004) The Tropospheric $^{14}CO_2$ Level in Mid-Latitudes of the Northern Hemisphere (1959–2003). *Radiocarbon* 46, 1261–1272. https://doi.org/10.1017/S0033822200033130

Lehmann, J., Kleber, M. (2015) The contentious nature of soil organic matter. *Nature* 528, 60–68. https://doi.org/10.1038/nature16069

Lützow, M.v., Kögel-Knabner, I., Ekschmitt, K., Matzner, E., Guggenberger, G., Marschner, B., Flessa, H. (2006) Stabilization of organic matter in temperate soils: mechanisms and their relevance under different soil conditions - a review. *European Journal of Soil Science* 57, 426–445. https://doi.org/10.1111/j.1365-2389.2006.00809.x

Manzoni, S., Katul, G.G., Porporato, A. (2009) Analysis of soil carbon transit times and age distributions using network theories. *Journal of Geophysical Research: Biogeosciences* 114, G04025. https://doi.org/10.1029/2009JG001070

Mathieu, J.A., Hatté, C., Balesdent, J., Parent, É. (2015) Deep soil carbon dynamics are driven more by soil type than by climate: a worldwide meta-analysis of radiocarbon profiles. *Global Change Biology* 21, 4278–4292. https://doi.org/10.1111/gcb.13012

Partin, C.A., Bekker, A., Planavsky, N.J., Scott, C.T., Gill, B.C., Li, C., Podkovyrov, V., Maslov, A., Konhauser, K.O., Lalonde, S.V., Love, G.D., Poulton, S.W., Lyons, T.W. (2013) Large-scale fluctuations in Precambrian atmospheric and oceanic oxygen levels from the record of U in shales. *Earth and Planetary Science Letters* 369–370, 284–293. https://doi.org/10.1016/j.epsl.2013.03.031

Petsch, S.T., Eglinton, T.I., Edwards, K.J. (2001) ^{14}C-Dead Living Biomass: Evidence for Microbial Assimilation of Ancient Organic Carbon During Shale Weathering. *Science* 292, 1127–1131. https://doi.org/10.1126/science.1058332

Possinger, A.R., Zachman, M.J., Enders, A., Levin, B.D.A., Muller, D.A., Kourkoutis, L.F., Lehmann, J. (2020) Organo–organic and organo–mineral interfaces in soil at the nanometer scale. *Nature Communications* 11, 6103. https://doi.org/10.1038/s41467-020-19792-9

Rosenheim, B.E., Galy, V. (2012) Direct measurement of riverine particulate organic carbon age structure. *Geophysical Research Letters* 39, L19703. https://doi.org/10.1029/2012GL052883

Schuur, E.A.G., Trumbore, S.E., Druffel, E.R.M., Southon, J.R., Steinhof, A., Taylor, R.E., Turnbull, J.C. (2016) Radiocarbon and the Global Carbon Cycle. In: Schuur, E.A.G., Druffel, E., Trumbore, S.E. (Eds.), *Radiocarbon and Climate Change: Mechanisms, Applications and Laboratory Techniques*. Springer, Cham, 1–19. https://doi.org/10.1007/978-3-319-25643-6_1

Shi, Z., Allison, S.D., He, Y., Levine, P.A., Hoyt, A.M., Beem-Miller, J., Zhu, Q., Wieder, W.R., Trumbore, S., Randerson, J.T. (2020) The age distribution of global soil carbon inferred from radiocarbon measurements. *Nature Geoscience* 13, 555–559. https://doi.org/10.1038/s41561-020-0596-z

Sierra, C.A., Müller, M., Metzler, H., Manzoni, S., Trumbore, S.E. (2017) The muddle of ages, turnover, transit, and residence times in the carbon cycle. *Global Change Biology* 23, 1763–1773. https://doi.org/10.1111/gcb.13556

Soil Survey Staff (2014) Illustrated Guide to Soil Taxonomy, Version 1.0. U.S. Department of Agriculture, Natural Resources Conservation Service, National Soil Survey Center, Lincoln, Nebraska, 552 p.

Torn, M.S., Trumbore, S.E., Chadwick, O.A., Vitousek, P.M., Hendricks, D.M. (1997) Mineral control of soil organic carbon storage and turnover. *Nature* 389, 170–173. https://doi.org/10.1038/38260

Trumbore, S.E., Zheng, S. (1996) Comparison of Fractionation Methods for Soil Organic Matter ^{14}C Analysis. *Radiocarbon* 38, 219–229. https://doi.org/10.1017/S0033822200017598